IEEE Access
Multidisciplinary | Rapid Review | Open Access Journal

Received July 27, 2021, accepted August 16, 2021, date of publication August 19, 2021, date of current version August 30, 2021.

Digital Object Identifier 10.1109/ACCESS.2021.3106227

Fabrication and Characterization of an 8 × 8 Terahertz Photoconductive Antenna Array for Spatially Resolved Time Domain Spectroscopy and Imaging Applications

RAPHAEL HENRI[1], KATHIRVEL NALLAPPAN[1], (Member, IEEE), DMITRY S. PONOMAREV[2,3], HICHEM GUERBOUKHA[4], DENIS V. LAVRUKHIN[2], ALEXANDER E. YACHMENEV[2], RUSTAM A. KHABIBULLIN[2], AND MAKSIM SKOROBOGATIY[1], (Senior Member, IEEE)

[1]Département de Génie Physique, Polytechnique Montréal, Montreal, QC H3C 3A7, Canada
[2]V.G. Mokerov Institute of Ultra High Frequency Semiconductor Electronics of the Russian Academy of Sciences, 117105 Moscow, Russia
[3]Prokhorov General Physics Institute of the Russian Academy of Sciences, 119991 Moscow, Russia
[4]School of Engineering, Brown University, Providence, RI 02912, USA

Corresponding author: Maksim Skorobogatiy (maksim.skorobogatiy@polymtl.ca)

This work was supported in part by the Canada Research Chair Tier I in Ubiquitous Terahertz Photonics, and in part by the Russian Science Foundation under Grant 18-79-10195.

ABSTRACT Terahertz (THz) technology is promising in several applications such as imaging, spectroscopy and communications. Among several methods in the generation and detection of THz waves, a THz time-domain system that is developed using photoconductive antennas (PCA) as emitter and detector presents several advantages such as simple alignment, low cost, high performance etc. In this work, we report the design, fabrication and characterization of a 2-D PCA array that is capable of detecting both the amplitude and phase of the THz pulse. The PCA array is fabricated using LT-GaAs and has 8 channels with 64 pixels (8 × 8). A novel approach using a spatial light modulator (SLM) to steer and focus the infrared probe beam towards pixels of the PCA array is presented. Each channel records the photocurrent generated by the THz signal (amplitude and phase) separately and frequencies up to 1.4 THz can be detected. Furthermore, the parameters such as directional time delay of the THz pulse, crosstalk between the channels etc., were characterized. Finally, we show that the proposed 2D PCA array design is flexible and can be used for accelerated THz spectral image acquisition.

INDEX TERMS Multipixel detector, photoconductive antenna array, terahertz imaging, THz time-domain system.

I. INTRODUCTION

Terahertz (THz) frequency band (0.1 to 10 THz) has received a lot of attention in recent years due to increasing number of technological applications in the fields of telecommunications, imaging and sensing [1]–[7]. Due to its non-ionizing nature and higher penetration depth when compared to optical infrared (IR) waves, the THz imaging is promising in such applications as security screening [8]–[10], biomedical imaging [11]–[16] and industrial process control [17], [18]. Moreover, the THz waves feature higher spatial resolution when compared to microwaves which attracted development of commercial THz imaging systems [19].

The THz imaging systems can be classified into two types: continuous wave (CW) THz imaging systems and pulsed THz time-domain imaging systems. The CW THz imaging systems offer compact, cost-effective, and relatively high power (compared to the THz time-domain systems) solutions for industrial applications in which a THz image at a given frequency can be obtained via raster scanning using a photomixer or Schottky detector [20], [21]. Although the CW THz system has higher frequency resolution (∼100 MHz) compared to a pulsed THz system, it requires a long acquisition time (several minutes per pixel depending on the

The associate editor coordinating the review of this manuscript and approving it for publication was Xihua Zou.

integration time and frequency resolution) to obtain a wide frequency spectrum with high signal to noise ratio, which limits its application in the fields of multi/hyperspectral imaging and real-time imaging. Moreover, emitters for CW THz imaging system in the form of photomixers are considerably more expensive than photoconductive antennas used in pulsed THz time domain systems. On the other hand, the THz time-domain system is the most commonly used imaging system as it allows recording a broadband THz pulse in a single acquisition sweep, with the following full spectrum reconstruction via Fourier transform of a time domain pulse. In such systems, the duration of the THz pulse acquisition is mainly limited by the sweeping speed of the optical delay line (typically in the form of a linear micro-positioning stage), as well as integration time that controls a signal to noise ratio. In the THz time-domain systems, the frequency resolution is typically on the order of ∼10 GHz, and while finer resolutions are readily achievable ∼1 GHz, they require higher values of optical delay (longer scanning ranges of a mechanical stage), thus resulting in longer image acquisition times. Similarly, smaller mechanical displacements of the optical delay stage are necessary in order to increase the upper frequency limit of the reconstructed THz spectrum, which again results in longer acquisition times. Several solutions have been proposed to decrease the acquisition time of the THz time-domain system such as asynchronous sampling [22], [23], fast rotary optical delay line [24], oscillating optical delay lines [25], etc. However, even if faster techniques for optical delay scanning are used, as the power in THz time-domain system is spread over a large frequency band, such systems tend to be noisier than the CW THz systems, thus requiring longer integration times. In the context of this work, the key advantage of the pulsed THz time domain approach compared to CW THz approach is the ability of integrating many photoconductive antennas on a single chip, which is in stark contrast to photomixers, which are technologically more difficult to fabricate and are currently available only as stand-alone devices.

The image acquisition speed in THz time-domain systems is also limited by the necessity of 2D raster scanning using a single pixel detector such as a PCA [26], a non-linear crystal [27], [28] or Air-based-coherent-detectors (ABCD) [29]. By employing mechanical beam steering [30], [31] or compressed sensing techniques such as phase mask encoding [32], spectral/temporal encoding [33], etc., the image acquisition speed can be improved even when using a single pixel detector [34].

To further improve the image acquisition speed in THz time-domain systems, the multipixel detectors such as bolometer arrays [35] and Complementary Metal Oxide Semiconductor (CMOS) cameras [36] are proposed. In these approaches, only the amplitude of the THz electric field is detected, while phase information is lost. In practical applications, however, phase information is highly desirable as it allows direct measurement of the material's dielectric constant and/or sample geometry [33].

One of the promising techniques to increase the image acquisition speed and simultaneously to record both amplitude and phase information is to use the PCA arrays. In 2002, Herrmann *et al.*, proposed and demonstrated the first 1D PCA array with 8 antenna elements separated by 500 μm each [37]. The antenna was fabricated using low-temperature grown GaAs (LT-GaAs), while particular attention was given to the receiver electronics in which the authors used alternate pulse locked gated integrator (APOGI) by replacing the commercial multichannel lock-in amplifiers. In 2008, Pradarutti *et al.*, demonstrated the 1D PCA array by increasing the number of antenna elements to 16 [38]. There, the efficiency of the PCA array was improved by illuminating the probe beam using microlens array and by simultaneously measuring the THz pulse from all the antenna elements. They further increased the number of antenna elements to 128 (1-D) in the following work [39]. In 2014, Brahm *et al.*, demonstrated the fabrication of a 1D PCA array (15 antenna elements) [40] using InGaAs/InAlAs multi-layer heterostructure substrate for the excitation wavelength of 1030 nm. All these works show that the fabrication of multipixel PCA array is promising for the development of high-speed THz imaging system. However, most of the systems discussed above use simultaneous illumination of the whole array with a high-power probing light, also requiring a microlens array for focusing the probing IR light onto the individual photoconductive antennas. The incorporation of a microlens array is an additional step in the fabrication process which further complicates the PCA chip design, while the necessity of using pulsed IR sources powerful enough to interrogate all the pixels simultaneously might considerably increase system costs. Moreover, by using the microlens array, the chance of cross-talk between the neighboring pixels is high as probing IR beams interrogate all the pixels simultaneously. Additionally, complex wiring required to access every PCA element in the array further complicates design of such chips and require novel solutions.

In order to increase sensitivity of the PCA-based arrays, plasmonic nano-antenna arrays were proposed. Thus, in 2016, Yardimci *et al.* reported a large area detector with a high THz sensitivity (dynamic range of ∼90 dB), and broadband operation range (∼5 THz) [41]. In 2020, Li *et al.*, presented a 63-pixel (9 × 7) focal plane array of plasmonic nano-antennas [42]. They achieved detection bandwidth of more than 2 THz for all their pixels with the signal-to-noise ratio greater than 60 dB. The main challenge with their design is the complexity of the readout circuit since each pixel was interrogated sequentially. Particularly, they used 4 multiplexers and a FPGA development board to route the THz signal from 63 pixels to a single transimpedance amplifier and a commercial single channel lock-in amplifier. Therefore, they could only read 1 pixel at the time resulting in slower THz image acquisition speed.

In this article, we present the design, fabrication and characterization of an 8-channel array of 8 × 8 PCA antennas (64 pixels) with a goal of its further applications in real-time THz spectral imaging. The 2D PCA array was fabricated

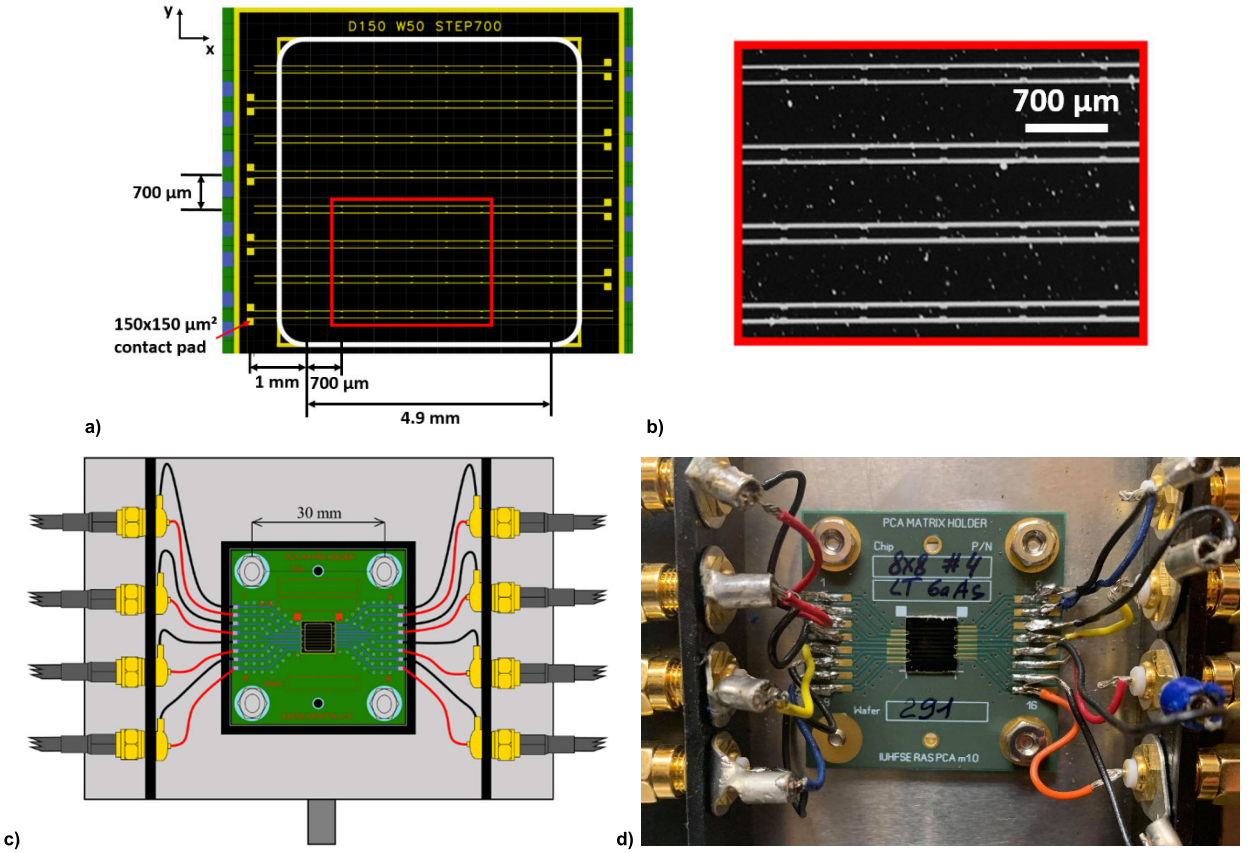

FIGURE 1. PCA detector array for THz time-domain imaging system. a) Schematic of the 8 × 8 PCA array. b) Microscope image of a part of the complete array showing 4 channels with 5 PCAs each c) Schematic of the PCB and holder assembly for the PCA array d) Photograph of the PCA array detector mounted on the PCB.

using LT-GaAs and its performance was characterized within the THz time-domain operation modality. A spatial light modulator (SLM) is used to form the wavefront of a probing IR beam by focusing it onto a single or multiple (chosen at will) PCA antenna elements. This novel approach for PCA array interrogation comes with multiple advantages. One of them is non-mechanic fast optical beam steering with the possibility of using multiple focal spots in order to interrogate multiple antennas simultaneously. In this case, antennas are grouped into separate channels (in our case 8 channels) that can be interrogated in parallel (i.e. by using 'N' transimpedance amplifiers for 'N' number of channels), thus speeding up image acquisition, and dramatically simplifying the on-chip wiring. Moreover, using SLM for interrogation allows smart power budget allocation depending on the total available power of the light source. For example, the number of pixels interrogated in parallel (hence, the number of focal spots generated by SLM) can be increased at the software level when using higher power pulsed IR lasers. At the same time, for a low power laser, one can use just a single beam spot (sequential pixel readout). Furthermore, by combining the proposed technique with the fast optical delay scanning [24] (rotary delay line for example [43]), the image acquisition speed can be further improved.

II. DESIGN AND FABRICATION OF THE THz PHOTOCONDUCTIVE ANTENNA ARRAY

The schematic of the proposed PCA arrays is shown in Fig. 1 (a). The array is comprised of 8 × 8 dipole H-type PCAs featuring a 100 μm photoconductive gap. The distance between two neighboring electrodes is 150 μm, the area of contact pads is 150 × 150 μm^2. The PCA array was fabricated in two steps. The LT-GaAs was used as a photoconductive substrate. The 0.5 μm thick LT-GaAs was grown via molecular-beam epitaxy using Riber 32P system at 220°C on a semi-insulating GaAs (001) wafer (BEP III/V ratio ∼35). To improve the LT-GaAs characteristics [44] and isolate the photoconductor from the wafer, a 50 nm thick AlAs layer was sandwiched between the LT-GaAs and the wafer. The LT-GaAs was then annealed at 600°C within 20 min in the growth chamber.

Then, the PCA array was fabricated using an electron-beam lithography (EBL). The sample was dehydrated on the hotplate at 180°C and coated with 540 nm/250 nm thick Copolymer/PMMA 950K bilayer resist stack. The required pattern was exposed via Raith 150-TWO EBL system at 30 kV and developed in an IPA:DI water mixture (1:3) to provide a proper lift-off profile. Then, we used an oxygen plasma descum processing followed by HCl (1:5) solution pretreatment to remove the oxides from the surface of

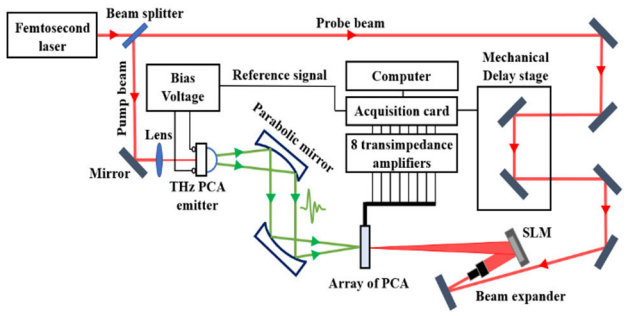

FIGURE 2. Schematic of the THz time-domain system for characterizing the PCA array. A spatial light modulator was used for focusing and steering the femtosecond laser beam on each PCA element of the array.

LT-GaAs. Finally, the 50 nm/450 nm thick Ti/Au metallization was deposited on the surface of LT-GaAs via resistive thermal evaporation. The fabrication routine of the single PCA in the array is similar to that reported in our previous paper [45], [46]. In Fig.1 (b), we present the microscope image of a part of the PCA array for the region marked in Fig.1 (a) showing 4 channels and 5 PCA elements each. The 6×6 mm^2 array was then mounted on a PCB board with a window for THz access on its backside as shown in Fig.1 (c-d).

On the PCB, there are 16 conductive tracks and each of them is connected to a contact pad. The two conductive tracks associated with one row of PCA are connected to a ring terminal with simple wires. A low noise cable with SMA and BNC connectors was then used to forward the signal towards the transimpedance amplifiers. This means that there are 8 detection channels and that each of them corresponds to a row of 8 PCA elements.

III. THz TIME-DOMAIN SYSTEM WITH SLM-DRIVEN PARALLELISED ACQUISITION

Schematic of the experimental setup used for characterization of the THz PCA array is shown in Fig. 2. A femtosecond laser with the center wavelength of 780 nm, average power of 63 mW, pulse duration of <100 fs and repetition rate of 100 MHz was used as the IR laser source. The laser beam was divided into pump and probe beam using a 70:30 beam splitter (∼19 mW for pump beam and ∼44 mW for probe beam) and a PCA from Menlo system [47] was used as the THz emitter. A variable optical attenuator was used to control the power of the pump beam and finally a 10 mW pump power was used for the excitation of the THz emitter. In the detector section, due to higher reflection losses in SLM, the available probe power was much lower (∼9 mW) for the excitation of the THz detector PCA array. Therefore, only a single spot was used (sequential pixel readout) during PCA interrogation. Two parabolic mirrors were used to collimate and focus the THz beam into the detector with the resultant THz beam spot roughly covering the entire 5mm × 5mm area of the PCA array. When compared with the standard THz time-domain system, the pump beam section (emitter side) is identical while the probe beam section (detector side) was modified for probing the PCA array. Particularly, a SLM (*Holoeye Pluto with 1920 × 1080 pixels*) [48] was used to steer and to focus the incoming expanded probe beam into the PCA array as shown in Fig. 2.

The spot size of the incident probe beam on the SLM was ∼8 mm which covers ∼1000 × 1000 pixels. The SLM was placed 30 cm away from the PCA array and a single focal spot size of ∼200 μm was achieved by displaying a Fresnel lens pattern on the SLM. It is also noted that the higher diffraction orders of the Fresnel lens pattern were ignored as they carry very low power and their influence in the characterization of PCA array was neglected. The main advantage of using SLM is that a multifocal spot can be trivially created to interrogate all 8 channels simultaneously, while the beam steering can be performed as fast as 60 Hz. Finally, the measured photocurrent from the 8 channels of the PCA array was amplified using 8 dedicated low-noise transimpedance amplifiers from *FEMTO* [49]. A high-speed data acquisition device from *National Instrument* was used to measure the reference signal and the output signals of the 8 transimpedance amplifiers. A multichannel virtual lock-in in *LabVIEW* was developed to extract both phase and amplitude information of the THz pulse. It is noted that, when a lock-in amplifier is used to detect a THz signal modulated at a frequency Ω, two components $E_X(t)$ and $E_Y(t)$ are obtained.

$$E_X(t) = \langle J(t, t') \cos(\Omega t') \rangle \quad (1)$$

$$E_Y(t) = \langle J(t, t') \sin(\Omega t') \rangle \quad (2)$$

where $J(t, t')$ is an instant photocurrent as measured using transimpedance amplifier at a time t' for a fixed optical delay value t. Average $\langle \ldots \rangle$ is a time integral over integration time t'. Here t is the time delay as provided by the optical delay line. By combining Eq. (1) and Eq. (2), we get a complex THz signal $E(t)$:

$$E(t) = E_X(t) + iE_Y(t) \quad (3)$$

The THz pulse amplitude in time domain is defined as *abs(E(t))*. In the Fourier space $E(\omega) = FFT(E(t))$, the spectral amplitude is defined as $abs(E(\omega))$, while phase is $arg(E(\omega))$. The above definitions for the THz amplitude and phase were used in the rest of the paper.

IV. CALIBRATION OF THE THz PHOTOCONDUCTIVE ANTENNA ARRAY

Before imaging, we perform two calibration steps of the PCA array. The goal of the fully automated calibration process is to locate the position of the 64 PCA elements in the reference frame of the SLM. By moving the center of the Fresnel lens pattern displayed on the SLM pixel by pixel in both spatial directions (X and Y directions), the focused laser probe beam is steered to scan the whole surface of the PCA array. Therefore, 64 positions of the Fresnel lens pattern on the SLM must be identified, which represent the different positions on the PCA array where maximum THz pulse amplitude is detected.

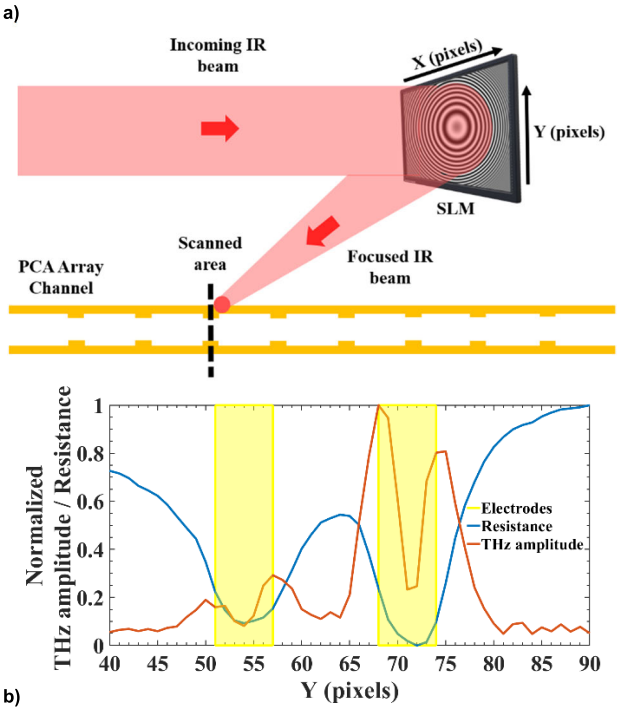

FIGURE 3. A single pixel (detector) characterization within an 8 × 8 PCA array a) Schematic of the probing beam path on the PCA array chip. The Fresnel lens pattern is used to focus and steer the laser probe beam of spot size ∼200 μm. b) Resistance and THz amplitude of the third PCA element of channel 5 which is measured by steering the laser probe beam along the Y-direction (see black dotted line shown in a). Two resistance drops are observed when the laser probe beam is focused directly on the metallic electrodes of the channel. Two THz pulses with higher amplitude were observed when the laser probe beam is focused on the edges of the metallic electrode associated with the positive terminal of the transimpedance amplifier and two THz pulses with lower amplitudes were observed while focusing at the edges of the negative terminal.

It is noted that the focal length of the Fresnel lens on the PCA array was optimized and remains fixed throughout the calibration process.

The first step in the calibration is to locate each channel of the detector array by measuring the drop in the channel resistivity via photoexcitation of the charge carriers in the gap between the two electrodes of a channel. Particularly, the resistance of a channel will drop drastically when the laser probe beam is focused near either one of the two electrodes of a channel. Thus, by steering the laser beam along the Y axis of the detector, one can easily identify the approximate position of each channel. The second step is to locate precisely where the THz pulse is detected with a maximal amplitude. By moving the laser probe beam across the PCA array and recording the THz signal for each position, it is possible to identify the exact location where the detection of the signal is optimal. As recording the THz pulse takes longer duration due to the slow scanning speed of the optical delay line used in our system, measuring of the channel resistance first provides a time efficient method to identify the region of interest on the PCA chip.

The schematic of the calibration process is shown in Fig.3 (a), where the incident laser probe beam on the SLM is focused onto the PCA array. One pixel in the SLM reference frame corresponds to 7μm distance in the PCA chip. This is identified based on the known dimensions of the PCA array (100 μm gap at the H-structure and 150 μm spacing between the electrodes). In Fig. 3 (b), we present the normalized value of the channel resistance, as well as the THz pulse amplitude as measured while scanning the IR laser beam across the black dotted line that traverses channel 5 as shown in Fig. 3 (a). We clearly observe two positions near the electrodes where the channel resistance drops, as well as four maxima in the recorded THz signal amplitude when focusing laser beam at the electrode edges. The amplitude of the THz pulse depends on the polarity of the electrode that is connected to the transimpedance amplifier. This was verified by reversing the polarity of the channel and observing the two highest THz amplitude peaks switching to the adjacent 2-peak group. This phenomenon can be explained by noting that in addition to the structure of the antenna, the lifetime and mobility of the charge carriers play a significant role in the detection of THz signal [50]. In LT-GaAs, the electron and hole carrier lifetimes are 0.1 ps and 0.4 ps, and the initial electron and hole mobilities are 200 cm^2/V s and 30 cm^2/V s respectively. Due to the difference in the lifetimes and mobilities of electrons and holes, the detection at the electrode that is connected to the positive terminal of the transimpedance amplifier will be predominant. This phenomenon is known for PCA emitters where the THz power is maximal when the laser beam is focused close to the anode [51]–[55].

The final step in the calibration process is to precisely locate the 8 antenna elements of each channel (2D) of the detector. As an example, the resistance map measured in the channel 5 of the PCA array as the region of interest is shown in Fig. 4 (a). Similarly, the two THz peaks associated with the electrode that is connected to the positive terminal of the transimpedance amplifier were measured and the corresponding THz amplitude map is shown in Fig. 4 (b). It should be noted that the amplitude of the THz pulse is smaller at the edges of the channel (X-direction) when compared to its center because of the lower power of the laser probe beam at the edges due to higher diffraction order of the Fresnel lens pattern and also due to the Gaussian distribution of the incident THz beam. We can also observe that THz signal is detected by all 8 H-gap antennas (A1 to A8). It is also interesting to note that while the detected THz signal is the strongest when focusing the probing IR beam within the H-gaps, the weaker THz signal can still be detected by focusing laser beam elsewhere along the electrode edge within the channel. In Fig. 4(c) we show time-resolved THz pulses acquired at the positions of the maximal THz amplitude as determined during the calibration procedure presented in Fig. 4 (b). The relative time delay between the THz pulses is due to different spatial positions of the corresponding acquisition locations along the channel. The ability of a 2D antenna array to measure spatial distribution of a pulse delay can be used

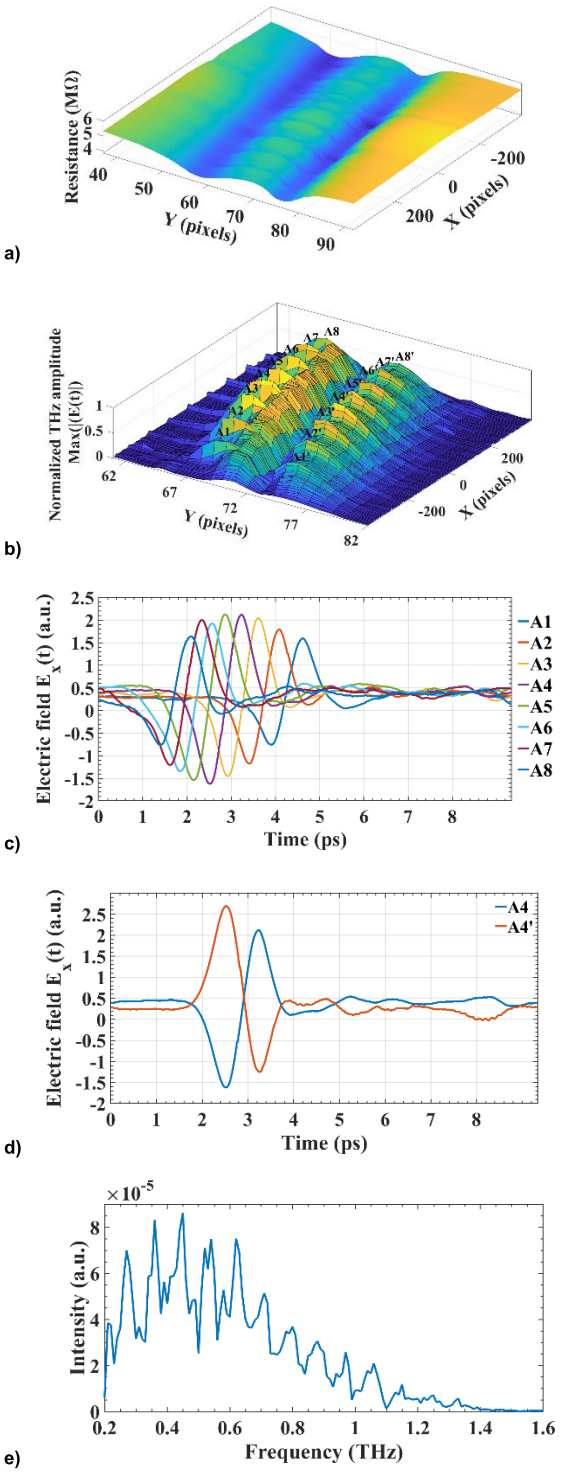

FIGURE 4. Channel characterization within an 8 × 8 PCA array. a) Resistance map for one of the channels (channel 5) in the array. The X and Y axis represent the position of the Fresnel lens center in the SLM reference frame. b) Amplitude of the THz pulse signal for the electrode that is connected to the positive terminal of the transimpedance amplifier (right electrode of the two seen in a)). c) THz pulses measured at the locations A1 to A8 as defined in b). d) THz pulse measured in the position A4 and A4′ as defined in b). e) Fourier Transform of the pulse recorded at A4.

for the THz radar applications to locate the direction and extrapolate the location of a THz light source.

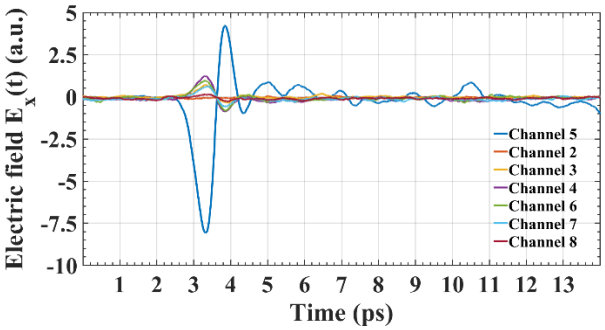

FIGURE 5. Inter-channel crosstalk within the PCA detector array. The laser beam is focused onto a single PCA element (#4) of the channel 5. The signals measured at the neighboring channels (2, 3, 4, 6, 7, and 8) are shown.

In Fig. 4 (d), we present the time-resolved THz pulses for the position A4 and A4' (4th antenna element of channel 5) as marked in Fig. 4 (b) which correspond to the laser beam being focused on either one of the two edges of the electrode that is connected to the positive terminal of the transimpedance amplifier.

In Fig. 4(e), we present the Fourier transform of one of the THz pulses measured with the array detector. The THz frequencies up to 1.4 THz can be detected. The oscillations in the spectrum can be explained by the Fabry-Perot effect due to resonances of the THz light inside the detector substrate. In a classical one-pixel PCA detector, a silicon lens is typically placed at the detector surface to focus the THz light into the antenna substrate, which also helps with decreasing the effect of standing waves. To reduce multiple reflections in the antenna array, an 8 × 8 micro-lens array could be designed to focus the THz light on each of the PCA detectors, or a THz antireflection coating can be used to optimize an array performance in the vicinity of a certain frequency, however, we defer further improvement to the array performance to our future work.

In array-based detectors, one of the major concerns is the channel crosstalk between the neighboring channels, which limits the sensitivity of the system. Therefore, in the following, we measure the crosstalk between the channels of the proposed PCA array. In order to estimate the channel crosstalk, the laser probe beam was focused into the fourth dipole antenna of the fifth channel located near the center of the PCA array. Then, the THz signal was measured at the neighboring channels as shown in Fig.5. From the figure we see that the maximal crosstalk of 15% (by field) is observed for the immediate neighboring channels (channel 4 and channel 6), while the crosstalk decreases rapidly for the channels that are further away. The channel crosstalk can be also minimized computationally after measuring all 64 spectrally resolved crosstalk matrices by exciting one antenna at a time and measuring crosstalk at the location of other antennas.

V. IMAGING USING THz PCA ARRAY

In order to use all the 8 channels of the detector for imaging, an array calibration is generally necessary. First, one must

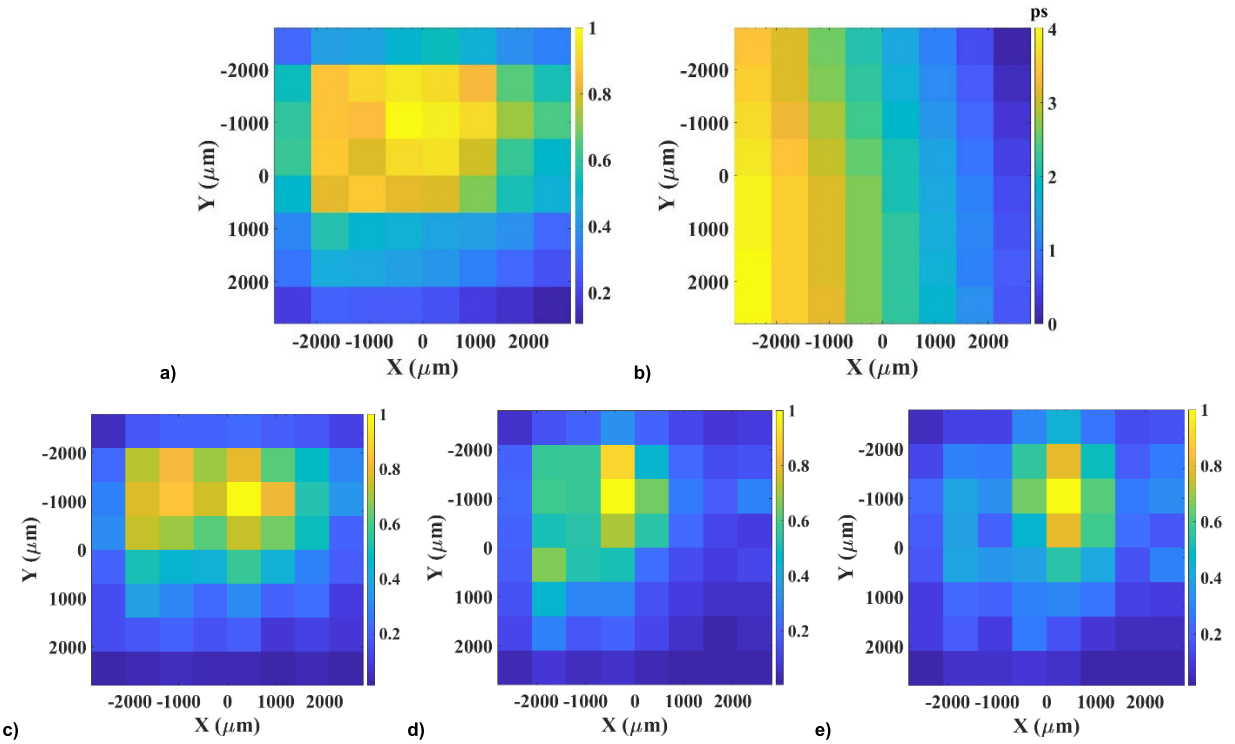

FIGURE 6. A reference image of the THz beam (empty system). a) Distribution of the maximal THz beam amplitude ($max(abs(E^{ref}_{c,p}(t)))$) of the time domain pulses as measured by the PCA array. b) Distribution of the relative time delay of the time domain THz pulses with respect to that measured by the top right pixel of the array. Spectral intensity distributions $I^{ref}_{c,p}(\omega)$ of the THz beam at different frequencies c) 0.29 THz, d) 0.44 THz, and e) 0.52 THz.

find the position of the 64 pixels (defined as locations of the local maxima in the THz amplitude), and then for each pixel (with indices $c = (1, 8)$ for the channel number, and $p = (1, 8)$ for the pixel number within a channel) record the complex reference THz pulses $E^{ref}_{c,p}(t)$ under illumination conditions that will be later used in imaging. Then, one would insert an object under study into the path of a THz beam and record a modified set of the THz pulses $E^{obj}_{c,p}(t)$. The complex spectral images of an object $S_{c,p}(\omega)$ (that include amplitude and phase information) can be retrieved by Fourier transforming the detected THz pulses and then dividing them by the complex spectral amplitudes of the reference pulses according to Eq.(4).

$$S_{c,p}(\omega) = \frac{E^{obj}_{c,p}(\omega)}{E^{ref}_{c,p}(\omega)} \tag{4}$$

In Fig. 6 (a), an example of a reference measurement is presented. There we show maximal amplitude distribution $max(abs(E^{ref}_{c,p}(t)))$ for the time domain THz pulses measured with the empty system. In Fig. 6 (b), we present the relative time delay of the THz pulses as registered by different pixels of an array compared to the top right pixel of the detector. The relative time delay is defined by comparing the temporal positions of the pulse amplitude maxima. A maximum time delay of 4 ps is observed with the bottom left pixel that is 6.9 mm farther away from the top right pixel. There are several reasons for a variable time delay across the PCA array including inclination of the measured THz beam wavefront, as well as variable distance between a SLM and the individual pixels as probed by the focused IR beam. The ability of measuring pulse delay distribution across the detector array paves the way to such advanced applications as full spatial characterization of the THz wavefront, distance ranging, THz incidence angle determination, etc., which we will explore in our future work. Although, the THz image obtained is pixelated (700 μm × 700 μm pixel size), the resolution could be improved by increasing the number of pixels along the channel since THz pulse can be detected even in between the H gaps as mentioned earlier. In Fig.6 (c-e), we present the spectral intensity distributions for the focused THz beam (by power) at different frequencies (0.29 THz, 0.44 THz and 0.52 THz), which are found by Fourier transforming the original data $I^{ref}_{c,p}(\omega) = (abs(E^{ref}_{c,p}(\omega)))^2$. It is then fitted using Gaussian beam profile (see Eq. (5)) along the X and Y direction. From Eq. (5), μ and σ are refers to mean and standard deviation of the Gaussian beam, respectively.

$$f(x, y) = \frac{1}{2\pi\sigma_X\sigma_Y} e^{-\left[\frac{(x-\mu_X)^2}{2\sigma_X^2} + \frac{(y-\mu_Y)^2}{2\sigma_Y^2}\right]} \tag{5}$$

The corresponding frequency dependent spot size ($FWHM_x = 2\sqrt{2ln2}\sigma_X$) are found to be 4.4 mm, 2.7 mm and 2.5 mm, respectively. The beam spot size decreases at

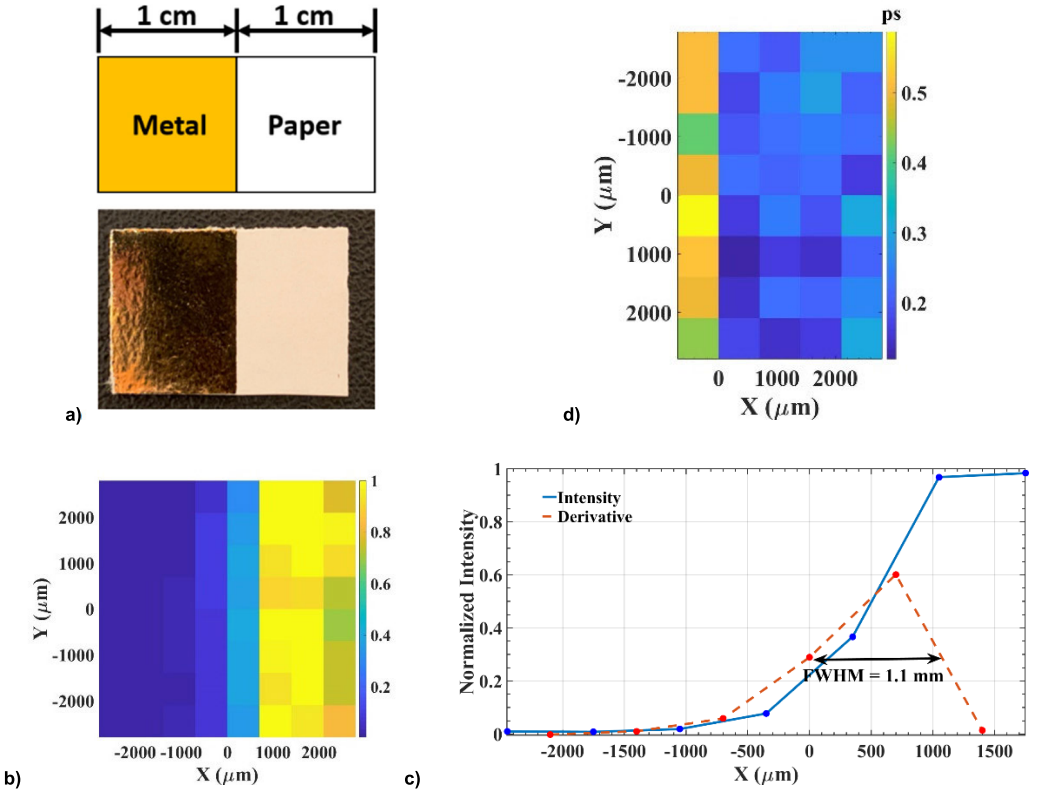

FIGURE 7. THz imaging of binary amplitude mask. a) Schematic and photograph of the binary amplitude mask which is fabricated using hot stamping technique. b) Relative intensity image of the THz time domain pulse. c) Average intensity along the X axis and its corresponding first-order derivative. d) The relative time shift of the THz pulse due to the presence of the paper sheet.

higher frequencies, which is consistent with the predictions of diffraction theory. From diffraction theory, the focal spot size $2w_0$ ($1/e^2$) for a lens of diameter D, focal length F and wavelength λ can be estimated using Eq. (6):

$$2w_0 = \left(\frac{4\lambda}{\pi}\right)\left(\frac{F}{D}\right) \tag{6}$$

In our THz time domain imaging system, the focal length and the diameter of the focusing optics (parabolic mirror) are 101.6 mm and 50.8 mm respectively. The FWHM ($2w_0 \cdot \sqrt{\ln(2)}/\sqrt{2}$) for the corresponding THz frequencies (0.29 THz, 0.44 THz and 0.52 THz) are then calculated as 1.56mm, 1mm and 0.87 mm, respectively. When comparing the results of FWHM, we see that values obtained in the experiment are somewhat larger than the ones predicted by the diffraction theory. This can be explained by various factors such as uncertainty in the position of the parabolic mirror focal plane, errors in the beam collimation, as well as multiple reflections in the substrate of a PCA array. It should be noted that for the same reasons, the center of the focal spot of the THz beam at different frequencies changes somewhat its position across the array.

To further demonstrate the abilities of a PCA array to perform amplitude and phase imaging, we carried out two experiments. In the first experiment, the object (sample) is a binary amplitude mask. It was fabricated by printing a thin metallic sheet on paper using hot stamping technique [56], [57]. The schematic and the photograph of the binary amplitude mask is shown in Fig. 7 (a). The sample was placed in front of the detector (stand-off distance between sample and detector is 3 mm due to PCB board thickness) with a metal sheet covering half of the pixels, and the rest of the pixels covered with a paper sheet. As mentioned earlier, a reference was taken with an empty system as shown in Fig.6 (a). By dividing the THz intensity (square of the electric field, $E_{c,p}^{obj}(t)^2$) measured with the sample by the intensity of the reference ($E_{c,p}^{ref}(t)^2$), we obtain Fig.7. (b). Clearly, a maximum amplitude is recorded when the THz light passes through the paper and no signal is recorded for the area covered by the metallic sheet. Moreover, the effect of diffraction on the metallic sheet edge is clearly visible near the center of the sample (metal/paper boundary). In Fig.7 (c), we present the normalized intensity profile along the X-axis of the THz image (see Fig.7 (b)) and its first-order derivative in order to estimate the resolution of the imaging system. The estimated FWHM of the derivative is ∼1.1 mm. Therefore, the resolution of the THz imaging system is ∼1.5 pixels (distance between two PCA element is 700 μm). Since the sample was placed 3 mm in front of the PCA array, the effect of diffraction reduces the resolution of the THz image to ∼1.5 pixels. However,

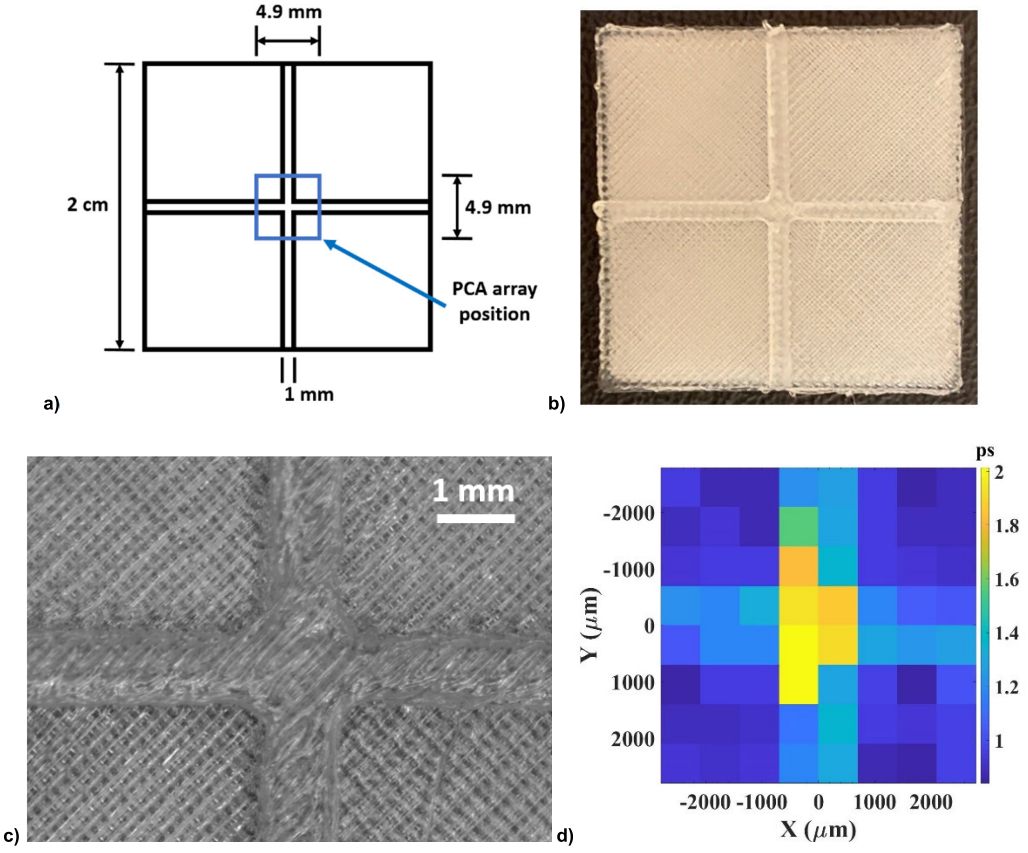

FIGURE 8. Relative time delay measurement of the phase mask. a) Schematic diagram of the phase mask (plastic cross). b) Photograph of the 3D printed phase mask c) Optical microscope image of the phase mask. d) The relative time delay of the THz pulse due to the presence of the phase mask as measured by the PCA array.

the resolution can be improved to 1-pixel by reworking the PCB integration and placing the sample closer to the PCA array. Finally, in Fig.7 (d), we present the relative time delay of the THz pulses when passing through the paper sheet as compared to the empty system (reference). As earlier, the relative time delay is defined by comparing the temporal positions of the pulse amplitude maxima for a system with and without a sample. An average time shift of $\Delta t{\sim}0.2$ ps was measured for the paper sheet. This is consistent with a simple estimate of $\Delta t = d\left(n_p - 1\right)/c{\sim}0.15$ ps relative pulse delay caused by the paper of 100μm thick with the refractive index (RI) of $n_p{\sim}1.45$ (see [58] for typical values of paper RI in THz).

In the second experiment, the sample is a phase mask which was fabricated using a 3D printing technique. A plastic cross with a thickness of 700μm was 3D printed on top of a 700μm thick substrate using a low loss polypropylene (PP) polymer. The length and the width of the plastic cross were 2 cm and 1 mm, respectively. In Fig.8 (a-c), we present the schematic, photograph and microscope image of the phase mask, respectively. The THz pulse was then recorded for each pixel and the relative time delay of the THz pulse as compared to an empty system (reference) is shown in Fig. 8(d). The shape of the cross is clearly recognizable from the time delay distribution caused by the spatially variable object thickness From a simple estimate we find that a 700μm thick PP slab (RI of bulk PP at THz is ∼1.49 [59]) should result in the relative time delay of ∼1.1 ps. However, due to porosity of the fabricated structure, the RI of 3D printed PP is lower than the bulk material, and is calculated to be ∼1.39 from the imaging data of Fig. 8(d). Thus, a relative time delay of ∼0.9 ps is registered for the porous substrate (700μm thick) of the phase mask and ∼1.8 ps for the plastic cross ($1400\ \mu$m thick), with the most optically dense part being in the cross center.

VI. CONCLUSION

In this work, we present the design, fabrication and characterization of a 2D 8 × 8 photoconductive antenna array for spatially resolved THz amplitude and phase imaging. First, the locations of optimal interrogation of the individual H-antennas in the detector array are mapped by steering the probe beam using Spatial Light Modulator. The inter-channel crosstalk is estimated to be as low as ∼15% (by field) for the adjacent channels. Then, calibration of the PCA array was performed by recording THz time traces for an empty system. Finally, we used a thus optimized and calibrated 2-D PCA array to demonstrate both amplitude and phase imaging.

For phase imaging, in particular, the relative THz pulse delay of both amplitude and phase mask was demonstrated. A somewhat suboptimal spatial resolution of ∼1.5 pixels was observed within amplitude imaging modality due to PCB thickness and suboptimal packaging that resulted in ∼3mm stand-off distance between samples and PCA array. A high-speed THz image acquisition can be achieved with this system due to 8-channel parallel data acquisition using virtual lock-in, as well as fast multi-beam steering capability of the SLM (60 Hz). The THz image acquisition speed can be further improved by combining high-speed SLMs (up to 2 KHz) [60] which are available commercially with the fast delay line techniques such as rotary optical delay line, oscillating optical delay line etc. Therefore, we believe that the proposed PCA array can be of practical importance in the development of next generation of real-time spectral imaging systems in the THz range.

ACKNOWLEDGMENT

(Raphael Henri and Kathirvel Nallappan contributed equally to this work.)

REFERENCES

[1] M. Beck, T. Plötzing, K. Maussang, J. Palomo, R. Colombelli, I. Sagnes, J. Mangeney, J. Tignon, S. S. Dhillon, G. Klatt, and A. Bartels, "High-speed THz spectroscopic imaging at ten kilohertz pixel rate with amplitude and phase contrast," *Opt. Exp.*, vol. 27, no. 8, pp. 10866–10872, 2019.

[2] C. M. Watts, D. Shrekenhamer, J. Montoya, G. Lipworth, J. Hunt, T. Sleasman, S. Krishna, D. R. Smith, and W. J. Padilla, "Terahertz compressive imaging with metamaterial spatial light modulators," *Nature Photon.*, vol. 8, no. 8, pp. 605–609, 2014.

[3] L. Zanotto, R. Piccoli, J. Dong, D. Caraffini, R. Morandotti, and L. Razzari, "Time-domain terahertz compressive imaging," *Opt. Exp.*, vol. 28, no. 3, pp. 3795–3802, 2020.

[4] T. Mohr, S. Breuer, G. Giuliani, and W. Elsäßer, "Two-dimensional tomographic terahertz imaging by homodyne self-mixing," *Opt. Exp.*, vol. 23, no. 21, pp. 27221–27229, 2015.

[5] H.-J. Song and T. Nagatsuma, "Present and future of terahertz communications," *IEEE Trans. THz Sci. Technol.*, vol. 1, no. 1, pp. 256–263, Sep. 2011.

[6] I. F. Akyildiz, J. M. Jornet, and C. Han, "Terahertz band: Next frontier for wireless communications," *Phys. Commun.*, vol. 12, pp. 16–32, Sep. 2014.

[7] D. M. Mittleman, "Twenty years of terahertz imaging," *Opt. Exp.*, vol. 26, no. 8, pp. 9417–9431, Apr. 2018.

[8] M. O. AlNabooda, R. M. Shubair, N. R. Rishani, and G. Aldabbagh, "Terahertz spectroscopy and imaging for the detection and identification of illicit drugs," in *Proc. Sensors Netw. Smart Emerg. Technol. (SENSET)*, 2017, pp. 1–4.

[9] J. Chen, Y. Chen, H. Zhao, G. J. Bastiaans, and X.-C. Zhang, "Absorption coefficients of selected explosives and related compounds in the range of 0.1–2.8 THz," *Opt. Exp.*, vol. 15, no. 19, pp. 12060–12067, 2007.

[10] H. Quast and T. Loffler, "Towards real-time active THz range imaging for security applications," in *Proc. Int. Conf. Electromagn. Adv. Appl.*, Sep. 2009, pp. 501–504.

[11] E.-M. Stübling, A. Rehn, T. Siebrecht, Y. Bauckhage, L. Öhrström, P. Eppenberger, J. C. Balzer, F. Rühli, and M. Koch, "Application of a robotic THz imaging system for sub-surface analysis of ancient human remains," *Sci. Rep.*, vol. 9, no. 1, Dec. 2019, Art. no. 3390.

[12] P. Doradla, K. Alavi, C. S. Joseph, and R. H. Giles, "Development of terahertz endoscopic system for cancer detection," *Proc. SPIE*, vol. 9747, May 2016, Art. no. 97470F.

[13] Q. Sun, Y. He, K. Liu, S. Fan, E. P. J. Parrott, and E. Pickwell-MacPherson, "Recent advances in terahertz technology for biomedical applications," *Quant. Imag. Med. Surg.*, vol. 7, no. 3, pp. 345–355, Jun. 2017.

[14] S. J. Park, S. H. Cha, G. A. Shin, and Y. H. Ahn, "Sensing viruses using terahertz nano-gap metamaterials," *Biomed. Opt. Exp.*, vol. 8, no. 8, pp. 3551–3558, 2017.

[15] T. C. Bowman, M. El-Shenawee, and L. K. Campbell, "Terahertz imaging of excised breast tumor tissue on paraffin sections," *IEEE Trans. Antennas Propag.*, vol. 63, no. 5, pp. 2088–2097, May 2015.

[16] R. Zhang, Q. Chen, K. Liu, Z. Chen, K. Li, X. Zhang, J. Xu, and E. Pickwell-MacPherson, "Terahertz microfluidic metamaterial biosensor for sensitive detection of small-volume liquid samples," *IEEE Trans. THz Sci. Technol.*, vol. 9, no. 2, pp. 209–214, Mar. 2019.

[17] G. Ok, K. Park, H. J. Kim, H. S. Chun, and S.-W. Choi, "High-speed terahertz imaging toward food quality inspection," *Appl. Opt.*, vol. 53, no. 7, pp. 1406–1412, 2014.

[18] X. Miao, H. Li, R. Bao, C. Feng, H. Wu, H. Zhan, Y. Li, and K. Zhao, "Discriminating the mineralogical composition in drill cuttings based on absorption spectra in the terahertz range," *Appl. Spectrosc.*, vol. 71, no. 2, pp. 186–193, Feb. 2017.

[19] K. Fukunaga, I. Hosako, I. N. Duling, III, and M. Picollo, "Terahertz imaging systems: A non-invasive technique for the analysis of paintings," *Proc. SPIE*, vol. 7391, Jul. 2009, Art. no. 73910D.

[20] M. Schiselski, M. Laabs, N. Neumann, S. Kovalev, B. Green, M. Gensch, and D. Plettemeier, "A planar Schottky diode based integrated THz detector for fast electron pulse diagnostics," in *IEEE MTT-S Int. Microw. Symp. Dig.*, May 2016, pp. 1–6.

[21] A. Roggenbuck, K. Thirunavukkuarasu, H. Schmitz, J. Marx, A. Deninger, I. C. Mayorga, R. Güsten, J. Hemberger, and M. Grüninger, "Using a fiber stretcher as a fast phase modulator in a continuous wave terahertz spectrometer," *J. Opt. Soc. Amer. B, Opt. Phys.*, vol. 29, no. 4, pp. 614–620, 2012.

[22] T. Yasui, E. Saneyoshi, and T. Araki, "Asynchronous optical sampling terahertz time-domain spectroscopy for ultrahigh spectral resolution and rapid data acquisition," *Appl. Phys. Lett.*, vol. 87, no. 6, Aug. 2005, Art. no. 061101.

[23] A. Bartels, R. Cerna, C. Kistner, A. Thoma, F. Hudert, C. Janke, and T. Dekorsy, "Ultrafast time-domain spectroscopy based on high-speed asynchronous optical sampling," *Rev. Sci. Instrum.*, vol. 78, no. 3, Mar. 2007, Art. no. 035107.

[24] H. Guerboukha, A. Markov, H. Qu, and M. Skorobogatiy, "Time resolved dynamic measurements at THz frequencies using a rotary optical delay line," *IEEE Trans. THz Sci. Technol.*, vol. 5, no. 4, pp. 564–572, Jul. 2015.

[25] Y.-S. Jin, S.-G. Jeon, G.-J. Kim, J.-I. Kim, and C.-H. Shon, "Fast scanning of a pulsed terahertz signal using an oscillating optical delay line," *Rev. Sci. Instrum.*, vol. 78, no. 2, Feb. 2007, Art. no. 023101.

[26] N. M. Burford and M. O. El-Shenawee, "Review of terahertz photoconductive antenna technology," *Opt. Eng.*, vol. 56, no. 1, Jan. 2017, Art. no. 010901.

[27] J. Hebling, K. L. Yeh, M. C. Hoffmann, and K. A. Nelson, "High-power THz generation, THz nonlinear optics, and THz nonlinear spectroscopy," *IEEE J. Sel. Topics Quantum Electron.*, vol. 14, no. 2, pp. 345–353, Mar. 2008.

[28] Z. Yang, L. Mutter, M. Stillhart, B. Ruiz, S. Aravazhi, M. Jazbinsek, A. Schneider, V. Gramlich, and P. Günter, "Large-size bulk and thin-film stilbazolium-salt single crystals for nonlinear optics and THz generation," *Adv. Funct. Mater.*, vol. 17, no. 13, pp. 2018–2023, Sep. 2007.

[29] X. Lu and X.-C. Zhang, "Balanced terahertz wave air-biased-coherent-detection," *Appl. Phys. Lett.*, vol. 98, no. 15, Apr. 2011, Art. no. 151111.

[30] K.-I. Maki and C. Otani, "Terahertz beam steering and frequency tuning by using the spatial dispersion of ultrafast laser pulses," *Opt. Exp.*, vol. 16, no. 14, pp. 10158–10169, 2008.

[31] N. Llombart, K. B. Cooper, R. J. Dengler, T. Bryllert, and P. H. Siegel, "Confocal ellipsoidal reflector system for a mechanically scanned active terahertz imager," *IEEE Trans. Antennas Propag.*, vol. 58, no. 6, pp. 1834–1841, Jun. 2010.

[32] H. Guerboukha *et al.*, "Super-resolution orthogonal deterministic imaging technique for terahertz subwavelength microscopy," *ACS Photon.*, vol. 7, no. 7, pp. 1866–1875, 2020.

[33] H. Guerboukha, K. Nallappan, and M. Skorobogatiy, "Exploiting k-space/frequency duality toward real-time terahertz imaging," *Optica*, vol. 5, no. 2, pp. 109–116, 2018.

[34] H. Guerboukha, K. Nallappan, and M. Skorobogatiy, "Toward real-time terahertz imaging," *Adv. Opt. Photon.*, vol. 10, no. 4, pp. 843–938, Dec. 2018.

[35] J. Oden, J. Meilhan, J. Lalanne-Dera, J.-F. Roux, F. Garet, J.-L. Coutaz, and F. Simoens, "Imaging of broadband terahertz beams using an array of antenna-coupled microbolometers operating at room temperature," *Opt. Exp.*, vol. 21, no. 4, pp. 4817–4825, 2013.

[36] I. E. Carranza, J. P. Grant, J. Gough, and D. Cumming, "Terahertz metamaterial absorbers implemented in CMOS technology for imaging applications: Scaling to large format focal plane arrays," *IEEE J. Sel. Topics Quantum Electron.*, vol. 23, no. 4, pp. 1–8, Jul. 2017.

[37] M. Herrmann, M. Tani, K. Sakai, and M. Watanabe, "Towards multi-channel time-domain terahertz imaging with photoconductive antennas," in *Proc. Int. Topical Meeting Microw. Photon. (MWP)*, 2002, pp. 1–4.

[38] B. Pradarutti, R. Müller, W. Freese, G. Matthäus, S. Riehemann, G. Notni, S. Nolte, and A. Tünnermann, "Terahertz line detection by a microlens array coupled photoconductive antenna array," *Opt. Exp.*, vol. 16, no. 22, pp. 18443–18450, 2008.

[39] A. Brahm, B. Pradarutti, S. Scharnowski, C. Bruckner, S. Riehemann, S. Nolte, G. Notni, and A. Tunnermann, "128 channel THz ultrashort pulse system," in *Proc. 34th Int. Conf. Infr., Millim., THz Waves*, Sep. 2009, pp. 1–2.

[40] A. Brahm, A. Wilms, R. J. Dietz, T. Göbel, M. Schell, G. Notni, and A. Tünnermann, "Multichannel terahertz time-domain spectroscopy system at 1030 nm excitation wavelength," *Opt. Exp.*, vol. 22, no. 11, pp. 12982–12993, 2014.

[41] N. T. Yardimci and M. Jarrahi, "High sensitivity terahertz detection through large-area plasmonic nano-antenna arrays," *Sci. Rep.*, vol. 7, no. 1, pp. 1–8, May 2017.

[42] X. Li and M. Jarrahi, "A 63-pixel plasmonic photoconductive terahertz focal-plane array," in *IEEE MTT-S Int. Microw. Symp. Dig.*, Aug. 2020, pp. 91–94.

[43] M. Skorobogatiy, "Linear rotary optical delay lines," *Opt. Exp.*, vol. 22, no. 10, pp. 11812–11833, 2014.

[44] A. Jooshesh, F. Fesharaki, V. Bahrami-Yekta, M. Mahtab, T. Tiedje, T. E. Darcie, and R. Gordon, "Plasmon-enhanced LT-GaAs/AlAs heterostructure photoconductive antennas for sub-bandgap terahertz generation," *Opt. Exp.*, vol. 25, no. 18, pp. 22140–22148, 2017.

[45] D. V. Lavrukhin, A. E. Yachmenev, I. A. Glinskiy, R. A. Khabibullin, Y. G. Goncharov, M. Ryzhii, T. Otsuji, I. E. Spector, M. Shur, M. Skorobogatiy, K. I. Zaytsev, and D. S. Ponomarev, "Terahertz photoconductive emitter with dielectric-embedded high-aspect-ratio plasmonic grating for operation with low-power optical pumps," *AIP Adv.*, vol. 9, no. 1, Jan. 2019, Art. no. 015112.

[46] D. V. Lavrukhin, A. E. Yachmenev, A. Y. Pavlov, R. A. Khabibullin, Y. G. Goncharov, I. E. Spektor, G. A. Komandin, S. O. Yurchenko, N. V. Chernomyrdin, K. I. Zaytsev, and D. S. Ponomarev, "Shaping the spectrum of terahertz photoconductive antenna by frequency-dependent impedance modulation," *Semicond. Sci. Technol.*, vol. 34, no. 3, Mar. 2019, Art. no. 034005.

[47] MenloSystems. (2019). *TERA8-1 THz-Antennas for 800 nm*. Accessed: Apr. 15, 2020. [Online]. Available: https://www.menlosystems.com/assets/datasheets/THz-Time-Domain-Solutions/MENLO_TERA8-1-D-EN_2019-12_3w.pdf

[48] Holoeye. (2021). *PLUTO-2.1 LCOS Spatial Light Modulator Phase Only (Reflective)*. [Online]. Available: https://holoeye.com/slm-pluto-phase-only/

[49] FEMTO. (2021). *Low-Frequency Voltage Amplifiers Series DLPVA*. [Online]. Available: https://www.femto.de/en/products/voltage-amplifiers/variable-gain-100-khz-dlpva.html

[50] J. Zhang, M. Tuo, M. Liang, X. Wang, and H. Xin, "Contribution assessment of antenna structure and in-gap photocurrent in terahertz radiation of photoconductive antenna," *J. Appl. Phys.*, vol. 124, no. 5, Aug. 2018, Art. no. 053107.

[51] G. Paz-Martínez, J. Garduño-Mejía, O. V. Kolokoltsev, C. G. Treviño-Palacios, and N. Qureshi, "Focus and alignment tolerance in a photoconductive terahertz source," *J. Infr., Millim., THz Waves*, vol. 36, no. 9, pp. 830–837, Sep. 2015.

[52] J. L. Carthy, P. C. Gow, S. A. Berry, B. Mills, and V. Apostolopoulos, "Terahertz focusing and polarization control in large-area bias-free semiconductor emitters," *J. Infr., Millim., THz Waves*, vol. 39, no. 3, pp. 223–235, Mar. 2018.

[53] M. J. Cliffe, A. Rodak, D. M. Graham, and S. P. Jamison, "Generation of longitudinally polarized terahertz pulses with field amplitudes exceeding 2 kV/cm," *Appl. Phys. Lett.*, vol. 105, no. 19, Nov. 2014, Art. no. 191112.

[54] I. S. Gregory, C. Baker, W. R. Tribe, I. V. Bradley, M. J. Evans, E. H. Linfield, A. G. Davies, and M. Missous, "Optimization of photomixers and antennas for continuous-wave terahertz emission," *IEEE J. Quantum Electron.*, vol. 41, no. 5, pp. 717–728, May 2005.

[55] S. E. Ralph and D. Grischkowsky, "Trap-enhanced electric fields in semi-insulators: The role of electrical and optical carrier injection," *Appl. Phys. Lett.*, vol. 59, no. 16, pp. 1972–1974, Oct. 1991.

[56] Y. Cao, K. Nallappan, H. Guerboukha, G. Xu, and M. Skorobogatiy, "Additive manufacturing of highly reconfigurable plasmonic circuits for terahertz communications," *Optica*, vol. 7, no. 9, pp. 1112–1125, 2020.

[57] H. Guerboukha, Y. Amarasinghe, R. Shrestha, A. Pizzuto, and D. M. Mittleman, "High-volume rapid prototyping technique for terahertz metallic metasurfaces," *Opt. Exp.*, vol. 29, no. 9, pp. 13806–13814, 2021.

[58] G. Yan, A. Markov, Y. Chinifooroshan, S. M. Tripathi, W. J. Bock, and M. Skorobogatiy, "Resonant THz sensor for paper quality monitoring using THz fiber Bragg gratings," *Opt. Lett.*, vol. 38, no. 13, pp. 2200–2202, 2013.

[59] Y.-S. Jin, G.-J. Kim, and S.-G. Jeon, "Terahertz dielectric properties of polymers," *J. Korean Phys. Soc.*, vol. 49, no. 2, pp. 513–517, 2006.

[60] U. B. Ljungblad, P. Askebjer, T. Karlin, T. Sandstrom, and H. Sjoeberg, "A high-end mask writer using a spatial light modulator," *Proc. SPIE*, vol. 5721, pp. 43–52, Jul. 2005.

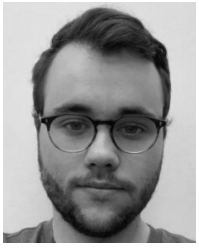

RAPHAEL HENRI received the B.Sc. degree in engineering physics from Polytechnique Montréal, Montreal, QC, Canada, in 2019, where he is currently pursuing the M.Sc. degree with Prof. Skorobogatiy, the Canada Research Chair Tier I in Ubiquitous Terahertz Photonics. His research interests include terahertz multipixels detector arrays, terahertz imagery, and terahertz time domain spectroscopy.

KATHIRVEL NALLAPPAN (Member, IEEE) received the B.E. degree in electronics and communication engineering and the M.Tech. degree in laser and electro-optical engineering from Anna University, Tamil Nadu, India, in 2010 and 2013, respectively, and the Ph.D. degree in terahertz communications from Polytechnique Montréal, Canada, in 2021. He was a Senior Project Fellow with the Structural Engineering Research Center, India, for a period of one year, he joined as a Research Intern with the Research Group of Prof. M. Skorobogatiy, Polytechnique Montréal. His research interests include terahertz and infrared free space communications, waveguide modeling, terahertz spectroscopy, and imaging.

DMITRY S. PONOMAREV received the M.Sc. degree in engineering physics from Moscow Engineering Physics Institute, in 2009, and the Ph.D. degree in physical and mathematical sciences from Moscow State Institute of Radio Engineering, Electronics and Automation, in 2012. He is currently the Deputy Director and an Associate Professor at V.G. Mokerov Institute of Ultra High Frequency Semiconductor Electronics of the Russian Academy of Sciences, and a Leading Researcher at Prokhorov General Physics Institute of RAS and V.G. Mokerov Institute of Ultra High Frequency Semiconductor Electronics of the Russian academy of Sciences, both Moscow, Russia. He does research in THz photonics, optoelectronics, and plasmonics. He mainly focuses on photoconductive devices for THz spectroscopy. He was awarded by the RAS, in 2018. In 2021, he became a laureate of the Annual Prize for the physicists by the Government of Moscow for his contribution to the development of photonics and optoelectronics THz devices.

HICHEM GUERBOUKHA received the B.Sc. degree in engineering physics, the M.Sc. degree in applied science, and the Ph.D. degree in engineering physics from Polytechnique Montréal, in 2014, 2015, and 2019, respectively. He is currently a Postdoctoral Research Fellow at the School of Engineering, Brown University. He is also currently a FRQNT Postdoctoral Research Fellow and working on THz communications. His previous research included THz instrumentation and waveguides, THz computational imaging, and THz communications. He was a recipient of the 2015 Releve Étoile Louis-Berlinguet from Fonds de recherche–Nature et technologies. He received the Best M.Sc. Thesis Award and the Best Ph.D. Thesis Award from Polytechnique Montréal, in 2015 and 2019, respectively.

DENIS V. LAVRUKHIN works as a Researcher at V.G. Mokerov Institute of Ultra High Frequency Semiconductor Electronics of the Russian Academy of Sciences, Moscow, Russia. He specializes in photoconductive THz device fabrication, pulse time-domain spectroscopy, and laser physics.

ALEXANDER E. YACHMENEV received the Ph.D. degree in physical and mathematical sciences from the Institute of Physics and Technology of the Russian Academy of Sciences, Moscow, Russia. He is currently a Senior Researcher at V.G. Mokerov Institute of Ultra High Frequency Semiconductor Electronics of the Russian Academy of Sciences, Moscow. He is leading the Molecular-Beam Epitaxy Group.

RUSTAM A. KHABIBULLIN received the M.Sc. degree in engineering physics from Moscow Engineering Physics Institute, in 2009, and the Ph.D. degree in physical and mathematical sciences from Moscow State Institute of Radio Engineering, Electronics and Automation in 2012. He is currently a Leading Researcher and an Associate Professor at V.G. Mokerov Institute of Ultra High Frequency Semiconductor Electronics of the Russian Academy of Sciences, Moscow, Russia. His research interests include THz technology and THz quantum-cascade lasers. He was awarded by the RAS, in 2018, and won the Annual Prize for the Physicists from the Government of Moscow, in 2021, for his contribution to the development of photonics and optoelectronics THz devices.

MAKSIM SKOROBOGATIY (Senior Member, IEEE) received the M.Sc. degree in electrical engineering and computer science and the Ph.D. degree in physics from MIT, in 2000 and 2001, respectively. He then served with the MIT spin-off OmniGuide Inc., where he was involved in the development of hollow-core fibers for guidance of high-power mid-IR laser beams. He has been a Professor of engineering physics with Polytechnique Montréal, since 2003. In 2017, he was an Elected Fellow of the Optical Society of America for his pioneering contributions to the development of micro-structured and photonic crystal multi-material fibers and their applications to light delivery, sensing, smart textiles, and arts. That same year, he was also promoted to a Senior Member of the IEEE for his contribution in engineering and applied research. He was awarded the Tier 2 Canada Research Chairs in Micro and Nano-Photonics, in 2005 and 2010, while in 2016, he was awarded a Tier 1 Canada Research Chair in Ubiquitous THz Photonics. The support from the Canada Research Chairs Program allowed him to pursue many high-risk exploratory projects in guided optics, smart materials, and recently THz photonics, which have resulted in significant contributions in these booming research fields. In 2012, he was awarded the rank of a Professional Engineer by the Order of Engineers of Quebec, Canada.